WILEY-VCH

DOI: 10.1002/ ((please add manuscript number))

Full Paper

p-type doped AlAsSb/GaSb resonant tunneling diode photodetector for the mid-infrared spectral region

Andreas Pfenning, Fabian Hartmann,** Robert Weih, Monika Emmerling, Lukas Worschech, and Sven Höfling*

Andreas Pfenning, Dr. Fabian Hartmann, Robert Weih, Monika Emmerling, Prof. Dr. Lukas Worschech, Prof. Dr. Sven Höfling
Technische Physik, Physikalisches Institut and Röntgen Center for Complex Material Systems (RCCM), Universität Würzburg, Am Hubland, D-97074 Würzburg, Germany
E-mail: andreas.pfenning@physik.uni-wuerzburg.de
E-mail: fabian.hartmann@physik.uni-wuerzburg.de

Prof. Dr. Sven Höfling
SUPA, School of Physics and Astronomy, University of St. Andrews, St. Andrews, KY16 9SS, United Kingdom

Keywords: ((resonant tunneling, GaSb, mid-infrared, photodetection, holes))

Mid-infrared (MIR) resonant tunneling diode (RTD) photodetectors based on a p-type doped AlAsSb/GaSb double barrier quantum well (DBQW) RTD are proposed and experimentally investigated for their optoelectronic transport properties. At room temperature, a distinct resonant tunneling current with a pronounced region of negative differential conductance (NDC) is measured. The peak-to-valley current ratio is $PVCR = 1.51$. To provide photosensitivity within the MIR spectral region, a lattice-matched quaternary low-bandgap GaInAsSb absorption layer with a cut-off wavelength of $\lambda = 2.77$ µm is integrated near the DBQW. Under illumination with infrared light, photogenerated minority electrons within the absorption layer can drift towards the DBQW, where they accumulate and cause a shift of the RTD current-voltage characteristics towards smaller bias voltages. The hole resonant tunneling current is modulated by optically generated electrons, which can be exploited to measure the incident MIR light power. In a tunable diode laser absorption spectroscopy experiment the RTD photodetector is used to identify three distinct water absorption lines in the MIR close to $\lambda =$

2.61 µm. By adjusting the absorption layer doping concentration, the RTD quantum efficiency can be increased by a factor of 10 resulting in a sensitivity of $S = 2.71$ A W^{-1}, which corresponds to an estimated multiplication factor of $M = 8.6$.

1. Introduction

Resonant tunneling diodes are versatile optoelectronic devices with a multitude of possible applications[1–3] ranging from fundamental research of noise correlations,[4–6] high-speed oscillators with operation frequencies in the THz regime,[7–9] and novel neuromorphic computation schemes[10,11] to highly-sensitive measurement devices of physical quantities such as strain,[12] temperature,[13] or light.[14–16]

In a recent publication, we proposed to apply the RTD photodetector principle to the mid-infrared (MIR) spectral region, by combining an antimony-based AlSb/GaSb double barrier quantum well DBQW resonant tunnelling structure (RTS) with an narrow bandgap absorption region.[17] Hereby, the RTD serves as an internal high-gain amplifier of small optically generated electrical signals. In contrast to, e.g. avalanche photodiodes where the gain is provided via impact ionization processes, the gain of RTD photodetectors originates from the modulation of a larger majority charge carrier tunnelling current that is sensitive to small variations of the local electrostatic potential.

The so called 6.1 Å family,[18] which is comprised of the three semiconductors InAs, GaSb, and AlSb offers a huge flexibility in designing electronic, optical and optoelectronic devices,[19] such as topological insulators,[20–23] optical MIR type-II superlattice photodetectors,[24] and quantum cascade lasers (QCL),[25–27] or interband cascade lasers (ICL),[27–31] and interband cascade detectors (ICD).[32,33]This flexibility can mainly be attributed to the huge variety of band line-ups, bandgap energies and in particular the so called InAs/GaSb type-II broken bandgap alignment. While the InAs/GaSb/AlSb material system has also brought forth a large variety of different resonant tunnelling structures,[3,18,34,35] only AlAsSb/GaSb RTDs provide

the required energy barriers in both valence and conduction band due to the type-I heterointerface.[36–39] In another recent publication, we demonstrated that room temperature resonant tunnelling of electrons in AlAsSb/GaSb RTDs requires the use of emitter prewells.[40–42] Here, we propose to invert the charge carrier polarity within the RTD photodetector, i.e. using p-type instead of n-type doping.

Using p-type doping in an RTD photodetector, and therefore hole instead of electron transport, might seem counterintuitive at first, since hole transport usually comes with several disadvantages. Due to their higher effective mass, holes have a lower mobility and a smaller De Broglie-wavelength compared to electrons.[43] A lower mobility results in inferior transport properties, a smaller De Broglie-wavelength demands a higher quality semiconductor crystal growth. However, and in particular for the GaSb material system, p-type doping may also offer several advantages: (i)Fermi-level pinning slightly above the valence band (VB), and the semi-metallic broken-bandgap InAs/GaSb interface allow for almost ideal Ohmic contacts.[44,45] (ii) GaSb already is intrinsically p-type doped with concentrations as high as $p \lesssim 10^{17}$ cm^{-3}. [46,47] In contrast to electrons in the conduction band (CB), holes remain at the Γ-point even at elevated temperatures,[43] making the otherwise required additional emitter prewell structures for room temperature operation no longer necessary.[40] (iii) A larger CB compared to VB offset of the absorption layer reduces a potential source of noise due to impact ionization and provides better confinement of photogenerated minority charge carriers (electrons).

Here, we present a detailed study on p-type doped AlAsSb/GaSb DBQW resonant tunneling diode photodetectors. Room temperature resonant tunneling of holes is observed with a peak-to-valley current ratio of up to $PVCR = 1.51$. By adding a lattice-matched and low-bandgap GaInAsSb absorption layer, photosensitivity within the mid-infrared (MIR) spectral region up to a cut-off wavelength of 2.77 µm is achieved and multiplication factors of $M = 8.6$ is shown.

2. Experimental Results

2.1. Sample Growth and Fabrication

The investigated samples are grown by molecular beam epitaxy (MBE) on a p-type Be-doped GaSb (100) substrate. After oxide desorption under Sb-stabilization flux at a substrate temperature of $T = 580$ °C, MBE growth starts. The first sample *RTD-p1* begins with 300 nm of p-type doped GaSb with $p = 1.5 \times 10^{18}$ cm^{-3}, followed by 20 nm of GaSb with a reduced doping concentration of $p = 0.2 \times 10^{18}$ cm^{-3}. Subsequently, the undoped resonant tunneling structure is grown, starting with 20 nm GaSb followed by two 4 nm wide lattice-matched $AlAs_{0.1}Sb_{0.9}$ barriers sandwiching a 3 nm wide GaSb quantum well. The RTS is capped by 15 nm GaSb and followed by 260 nm of the lattice-matched quaternary compound semiconductor $Ga_{0.76}In_{0.24}As_{0.20}Sb_{0.80}$. The first 30 nm of the absorption layer are left undoped, whereas the following 230 nm are doped with $p = 0.2 \times 10^{18}$ cm^{-3}. The growth is completed with a 300 nm thick GaSb layer with $p = 1.5 \times 10^{18}$ cm^{-3}.

The reference sample *RTD-p2* is largely identical to the sample described before, except for its completely undoped absorption region.

The doping profiles are examined and confirmed by time-of-flight secondary ion mass spectroscopy (TOF-SIMS). MBE growth rates and the thicknesses of the different semiconductor layer structures are examined and confirmed by cross-sectional scanning electron microscopy (SEM). **Figure 1 (a)** and **(b)** show SEM images of the layer structure of the grown RTD sample. Dark contrast represents higher Al concentrations, which allows for identifying width and position of the AlAsSb DBQW. ~~The SEM image indicates good crystal quality with no apparent dislocations or defects.~~ To illustrate the p-type RTD photodetection mechanism, the SEM images of Figure 1 (a) and (b) are overlain by the conduction (CB) and valence band (VB) profiles for an applied bias voltage of $V = -0.5$ V. Simulations of the CB and VB profiles are carried out using the *nextnano* simulation tool.[48] The CB profile is shown

as solid green line and the VB profile as solid red line. The $AlAs_{0.1}Sb_{0.9}$ double barrier height of $\Delta E_V \approx 0.49$ eV is calculated assuming a VB bowing parameter of zero. Please note that the composition-dependent material parameters of AlAsSb are not very well-researched and the actual barrier height might differ from the one we have calculated. When a negative bias voltage is applied to the top contact of the RTD, holes can tunnel resonantly via the first quantized heavy or light hole state of the DBQW RTD and are emitted from the GaSb substrate side. When the RTD is illuminated and the photon energy is greater than the bandgap energy of the narrow bandgap absorption region, electron-hole pairs will be excited under photon absorption. Photogenerated holes drift together with the conventional majority charge carriers towards the top contact due to the applied electrical field. The minority photogenerated electrons are captured for accumulation in the vicinity of the resonant tunneling structure. Due to their presence, the local electrical field is enhanced and the current-voltage characteristic shifts towards smaller voltages. This mechanism is similar to that in a phototransistor, and hence a minority of photogenerated electrons can modulate a larger resonant tunneling current of holes. Because in GaInAsSb the bandgap reduction happens almost exclusively in the CB, the antimonide system is especially apt for accumulation of electrons instead of holes.

After the growth process, circular RTD mesa structures with diameters from $d = 2$ µm up to $d = 14$ µm are defined by optical lithography. The structure transfer is done via a dry-chemical etching process. The etching depth is about 50 nm below the DBQW. The polymer BenzoCycloButene (BCB) is used for sidewall passivation. On the substrate side, an AuGe/Ni/Au contact is evaporated. On top of the RTD mesa structures, Ti/Au ring-shaped contacts are deposited. Figure 1 (c) shows a colored SEM image of the RTD mesa structure and the ring-shaped contact. The overlap between mesa and metal contact is clearly visible, as well as the open inner cut-out. This design allows for good electrical contact while simultaneously guaranteeing optical access. Besides the ring-shaped contact design alternative designs such as plasmonic hole arrays exist.[49]

2.2. Optical Characterization

The optical characteristics of the narrow-bandgap absorption layer are probed by Fourier-transform infrared (FTIR) photoluminescence (PL) spectroscopy. The PL spectrum was measured at a temperature of $T = 20$ °C, which corresponds to a thermal energy of $k_B T = 25$ meV, where k_B is Boltzmann's constant. The normalized PL spectrum is shown in **Figure 2 (a)**. The PL emission peak is located at an energy of $E_{Peak} \approx 0.47$ eV, which corresponds to a wavelength of $\lambda_{Peak} = 2.64$ µm. The full width at half maximum is $FHWM \approx 50$ meV and hence is $2 \cdot k_B T$. Because the PL spectrum is measured in ambient air, it is subject to water absorption lines, which are centered around λ_{Peak}.

The high-energy side of the spectrum follows Boltzmann's distribution function (light blue line, $\propto \exp(-h\nu/(k_B T))$, where h is Planck's constant and ν the photon frequency). The charge carriers are thermalized at the ambient temperature of $T = 20$ °C. On the low-energy side, the PL spectrum is determined by Urbach's rule, which states that due to the formation of bandtails photons with an energy lower than the bandgap energy ($h\nu < E_{gap}$) can also be absorbed or emitted. The intensity of absorption or emission, respectively, is $\propto \exp(h\nu/E_U)$, with the Urbach-parameter E_U.[50,51] The Urbach-parameter is a measure of structural and thermal disorder within the semiconductor material. From the fit function (see dashed red line, Figure 2 (a)), an Urbach-parameter of $E_U = 10$ meV is extracted. This compares well with previously reported values between $E_U = 5$ meV up to 10 meV for GaInAsSb grown by liquid phase epitaxy.[52] For comparison, the typical room temperature value for undoped GaAs is $E_{U,GaAs} = 7.5$ meV and Si-doping with $n = 2.0 \times 10^{18}$ will increase that value up to 13 meV.[53]

The position of the PL maximum is poorly suited to determine the bandgap energy. Urbach's rule describes the spectrum below the bandgap energy. The bandgap energy $E_G \cong$

(447 ± 5) meV is therefore determined by the point at which the PL spectrum deviates from the Urbach fit function as indicated by the orange arrow in Figure 2 (a). E_G corresponds to a cut-off wavelength of $\lambda_C = (2.77 \pm 0.04)$ µm.

E_{Gap} can furthermore be used to confirm the molar composition of the quaternary absorption layer. The condition for lattice-matched growth of GaInAsSb on GaSb is given by $(GaSb)_x(InAs_{0.91}Sb_{0.09})_{1-x}$.[43] **Figure 2 (b)** shows the bandgap energy as a function of x. The plotted data points (black spheres) are taken from *Shim*,[54] whereas the black line shows the cubic interpolation. The orange arrow indicates the bandgap energy as extracted from the PL spectrum and marks the position of $x = 0.76$, which confirms the grown composition of $Ga_{0.76}In_{0.24}As_{0.20}Sb_{0.80}$.

2.3. Optoelectronic Transport Characterization

2.3.1. Resonant Tunneling of Holes and Proof of Concept

To investigate the optoelectronic transport characteristics of the p-type doped RTD photodetector, the current-voltage (I(V)) characteristics of a diode with diameter $d = 12$ µm are measured in the dark and under excitation with laser light of the wavelength $\lambda = 1.30$ µm. All measurements are taken at room temperature.

Figure 3 shows the I(V)-characteristic in the dark (black) and under illumination (red) for positive and negative bias voltages and an incident light power of $P \lesssim 0.7$ mW. The resulting photocurrent-voltage characteristic (blue) is given by subtracting the I(V)-characteristic in the dark from the I(V)-characteristics under illumination, $I_{Ph}(V) = I_{illu}(V) - I_{dark}(V)$.

The I(V)-characteristic is symmetrical and at bias voltages of $V = -2.18$ V and $V = 1.62$ V, two distinct resonance currents of $I_{res} = -1.18$ mA and $I_{res} = 1.39$ mA followed by a region of negative differential conductance (NDC) can be observed. The corresponding peak-to-valley

current ratios are $PVCR = 1.52$ and $PVCR = 1.40$, respectively. The resonance currents can be ascribed to resonant tunneling of holes via the first quantized light hole state of the double barrier quantum well. The symmetric I(V)-characteristics can be ascribed to a symmetric VB profile (see Figure 1 (a) and (b)). The peak-to-valley current ratios are comparable to those observed in n-type AlAsSb/GaSb RTDs with ternary prewell emitters, which indicates high-quality crystal growth of the investigated diodes.[40] From further experimental studies of various RTDs with different diameters and temperatures, we can conclude that the fabrication and growth process provide an excellent yield and reproducibility (uniformity of the current density and resonance voltage position, no apparent sidewall leakage).

$I_{Ph}(V)$ is an asymmetric function of V. For positive bias voltages, I_{Ph} is strongly reduced compared to negative bias voltages. The asymmetry of $I_{Ph}(V)$ can be ascribed to the asymmetric semiconductor heterostructure with its low-bandgap absorption layer located at the top-side of the DBQW only (see Figure 1 (a) and (b)). It is a strong indicator of modulation of the resonant tunneling current due to charge carrier accumulation. Accumulation of photogenerated minority charge carriers (electrons) close to the DBQW occurs for negative bias voltages only. Due to the photon energy of $h\nu = 0.95$ eV, photon absorption and subsequent generation of electron hole pairs is also present outside the absorption layer within the GaSb emitter and collector regions. Thus, for positive bias voltages a non-zero photocurrent is measured. For larger negative bias voltages, the photocurrent increases, until a local maximum of $I_{Ph} \simeq 250$ µA is reached at $V = -1.05$ V. Further increasing of the reverse bias voltage leads to a drop of the photocurrent, which is ascribed to a reduced lifetime of photogenerated minority charge carriers.[55,56]

The p-type doped RTD photodetector is then excited with an MIR single-mode semiconductor diode laser from *nanoplus*. The laser emits at the wavelength of $\lambda = 2.6$ µm and can be used

for tunable diode laser absorption spectroscopy of water vapor. The laser is collimated by default and focused on the sample with a lens with a focal length of $f = 2.0$ cm.

To determine the fraction of the light power incident on the RTDs optical window, the RTD is operated at a constant voltage of $V = -0.8$ V and the photocurrent is measured, while the RTD is moved across the image plane (perpendicular to the optical axis) using piezo-stages. The minimum step size of the piezo stages is 100 nm. The resulting beam profile of the laser with the RTD in focus is shown in **Figure 4 (a)** as black spheres. The optically active area of the RTD is determined by scanning electron microscopy (see inset in Figure 4 (a)). The diameter of the ring-shaped contact optical window is $d = 8.14$ µm. Hence, the optical aperture is sufficiently small not to influence the measured beam profile. The photocurrent is directly proportional to the incident light power in the range of the irradiated intensities. Hence, the measured photocurrent reflects the actual beam profile. An extrapolation of the beam profile in polar coordinates and subsequent integration results in a fraction of maximal 5.8 % of the laser power being incident on the optical aperture.

After focusing the laser beam maximum on the sample, the I(V)-characteristics are measured again in the dark and under illumination (see **Figure 4 (b)**). The laser is operated at a constant temperature of $T = 30$ °C and at a constant current $I_{LD} = 115$ mA, which corresponds to an incident light power of $P \simeq 180$ µW on the ring contact's optical aperture. An extrinsic current bistability is observed with the threshold voltages of $V_{t1} = -3.31$ V and $V_{t2} = -3.10$ V. The bistability is caused by the load resistance of $R = 1.0$ kΩ.

When illuminated, the I(V)-characteristic shifts towards higher voltages (smaller absolute values of the reverse bias). The shift of the I(V)-characteristic can be ascribed to Coulomb interaction with accumulated photogenerated electrons.

Figure 4 (c) shows the photocurrent-voltage characteristics. For positive bias voltages, I_{Ph} is slightly above zero. In contrast to illumination with light of the wavelength of $\lambda = 1.3$ µm,

absorption is only present within the absorption layer. As a result, the photocurrent component for positive bias almost vanishes completely. The marginal residual component can be attributed to heating of the sample which inevitably occurs at incident light powers in the range of hundreds of µW.

For negative bias voltages, I_{Ph} initially rises to higher absolute values. A quantum efficiency threshold voltage cannot be observed. Due to the low VB discontinuity between GaInAsSb and GaSb (see Figure 1), the formation of a built-in potential preventing electron accumulation at the RTS is negligible. A local maximum of the absolute photocurrent of $I_{Ph} = -24$ µA is reached at at $V = -1.1$ V. This corresponds to a sensitivity of $S = 0.13$ A W^{-1}. After exceeding the local maximum, the absolute value of I_{Ph} continuously decreases and approaches zero. The measured I(V)-characteristics is distinctive for RTD photodetectors with a lower-bandgap energy absorption layer and for the modulation of a (resonant tunneling) current via Coulomb interaction.[14,55–59]

To demonstrate the capability of the p-type doped AlAsSb/GaSb RTD photodetector for optical molecule and gas spectroscopy, a TDLAS experiment on water vapor is performed. **Figure 5 (a)** shows the absorption spectrum of water vapor at a temperature of $T = 25$ °C within the spectral region at about $\lambda = 2.6$ µm. Three absorption lines are apparent within the spectral window at $\lambda = 2.6035$ µm, 2.6042 µm, 2.6056 µm, and 2.6076 µm. In the experiment, the RTD is excited with the wavelength-tunable diode laser. Increasing the laser current I_{LD} not only increases the output, it also leads to an increased internal Joule heating within the laser, which is accompanied by a red-shift of the laser emission wavelength.

The RTD is operated at a constant voltage of $V = -0.8$ V and I_{Ph} is measured as a function of the incident light power P. **Figure 5 (b)** shows the absolute photocurrent I_{Ph} as a function of the incident laser emission power on the optical aperture. I_{Ph} increases linearly with increasing P. When the emission wavelength crosses a water absorption line, the measured power drops

and distinct minima of the photocurrent can be observed that correspond to water absorption lines. For a known absorption coefficient α and distance covered by the laser light, the molecular concentration of the examined gas (here H_2O) can be determined by Lambert-Beer's law.

The measured sensitivity of $S = 0.13$ A W^{-1} seems unexpectedly low (see Figure 4 (c)). The sensitivity of RTD photodetectors is primarily determined by the RTD quantum efficiency η_{RTD}, the lifetime of photogenerated minority charge carriers τ.[55,56] Particularly with the high electron confinement potential, one would expect large electron lifetimes and associated sensitivities. In the following part, we demonstrate, how η_{RTD} and therefore the sensitivity S can be enhanced by carefully engineering the absorption layer doping profile. This study is achieved by a comparison of the optoelectronic transport properties of *RTD-p1* and the reference sample with undoped absorption region *RTD-p2*.

Figure 6 shows a comparison between the current density-voltage (j(V)) characteristic *RTD-p1* (black) and *RTD-p2* (red dashed line). The current density of *RTD-p2* is enhanced by a factor of about two compared to *RTD-p1*, which can be attributed to slightly thinner barriers or a slightly reduced As concentration of the AlAsSb barrier. Both j(V)-characteristics are comparable and show pronounced resonance currents for both, positive and negative bias voltages. For negative bias voltages, the resonance position of *RTD-p2* is shifted by $\Delta V \backsimeq 3.1$ V, from $V_{Res} = -2.3$ V to $V_{Res} = -5.4$ V compared to *RTD-p1*. The resonance current density is $j_{Res} = -20.8$ µA µm^{-2} and the corresponding peak-to-valley current ratio is $PVCR = 1.51$. In contrast, for positive bias voltages, the resonance voltage is only slightly shifted towards higher voltages by $\Delta V = 0.6$ V. The shift of the resonance current voltage is due to the altered doping profile of *RTD-p2*. The upper inset in Figure 6 shows numerical simulations of the VB profile for increasing absorption layer doping concentrations of the upper 230 nm from intrinsic to $p = 4.0 \times 10^{17}$ cm^{-3}. Lower doping concentrations result in a larger voltage drop across the

complete absorption layer. Hence, the RTD leverage factor is reduced. The parallel course of the j(V)-characteristics on the log-log scale (see lower right inset) confirms that the shift of the resonance voltage is due to a lower RTD leverage factor n_{RTD}. The RTD leverage factor is a figure of merit that quantifies how strong the applied bias voltage shifts the resonant tunneling energy level. n_{RTD} can be significantly stretched out due to band bending, especially when the collector spacer layer is large and the doping concentration is low.[60] The variation of the RTD leverage factor can be determined from the quotient of the resonance voltages to be $n_{RTD\text{-}p2} = 0.42 \cdot n_{RTD\text{-}p1}$, with $n_{RTD\text{-}p2}$ being the RTD leverage factor of *RTD-p2* and $n_{RTD\text{-}p1}$ being the RTD leverage factor of *RTD-p1*.

The reduction of n_{RTD} for decreasing doping of the absorption layer only occurs for negative voltages, i.e. in case of depletion. For positive bias voltages, holes are injected from the Au ring-shaped contact from where they drift within the applied electric field until they accumulate at the DBQW. The accumulated hole population at the DBQW then causes flat-band conditions within the absorption layer and hence the leverage factor remains unaffected.

To study the influence of the reduced absorption layer doping on the RTD photosensitivity, *RTD-p2* is excited with a laser of the wavelength $\lambda = 2.61$ µm analogous to *RTD-p1*.

Figure 7 shows the I(V)-characteristics for negative voltages measured in the dark (black) and under illumination (red). The incident power is $P \backsimeq 180$ µW. Under illumination, a well pronounced modulation of the I(V)-characteristic is apparent. $I_{dark}(V)$ is shifted to smaller absolute voltage values when illuminated. In comparison to *RTD-p1*, the modulation of the resonant tunneling current under illumination is significantly enhanced, which results in an increased photocurrent. The photocurrent-voltage ($I_{Ph}(V)$-) characteristic is also shown in Figure 7 (blue). $I_{Ph}(V)$ shows two local extrema of $I_{Ph} = -488$ µA at $V = -2.18$ V and $I_{Ph} = 620$ µA within the NDC region at $V = -5.7$ V. The photocurrent extrema correspond to sensitivities of $S = 2.71$ A W^{-1} and $S = 3.45$ A W^{-1}, respectively. Compared with *RTD-p1*, the

sensitivity is enhanced by a factor of 21. Approximately half of this is due to current density that is increased by a factor of 2. Therefore, the remaining factor of about 10 can be attributed to an increase of the RTD quantum efficiency.

By reducing the doping concentration of the upper 230 nm of the GaInAsSb absorption layer, flat band conditions are prevented. As a result, photogenerated electrons are captured effectively by the external field and drift towards the DBQW. The RTD multiplication factor $M = 8.6$ can then be estimated via $S = M \cdot \eta_{RTD} \cdot R_\lambda$, with the spectral responsivity at $\lambda = 2.61$ µm $R_\lambda = 2.10$ A W^{-1}. The RTD quantum efficiency of $\eta_{RTD} = 0.15$ is calculated for normal incidence considering an absorption coefficient of $\alpha = 1 \times 10^4$ cm^{-1} and only reflection at the air/semiconductor interface as loss factor.[61,62] The amplification is therefore about double the gain observed in interband cascade photodetectors.[63]

3. Conclusion

A novel photodetector concept that provides gain at relatively small operating voltages is proposed, demonstrated, and examined. The investigated samples are based on p-type doped AlAsSb/GaSb DBQW RTDs with an integrated quaternary GaInAsSb absorption layer. The investigated RTD photodetectors show a pronounced photosensitivity to illumination with MIR light and can therefore be used for molecule and gas sensing applications based on absorption spectroscopy. The photocurrent-voltage characteristic confirms that the photosensitivity within the p-type doped RTD photodetectors is due to the modulation of a resonant hole tunneling current via the Coulomb interaction by accumulated photogenerated minority charge carriers (electrons).

Sensitivities of $S = 0.13$ A W^{-1} are observed. The sensitivity can be further enhanced up to $S = 2.71$ A W^{-1} by an optimized absorption layer doping profile. The optimized doping profile results in an increased quantum efficiency at the cost of a reduced RTD leverage factor. We

expect that the multiplication factor can be enhanced by at least one order of magnitude by reducing the buffer layer thickness from 15 nm to 1 nm.

In a demonstration experiment, gas absorption spectroscopy of water vapor is conducted at three consecutive water absorption lines using the RTD as MIR photodetector.

In conclusion, we have demonstrated room temperature resonant tunneling of holes in a GaSb/AlAsSb double barrier quantum well resonant tunneling structure and studied its transport characteristics across a broad temperature range. This structure is an important building block for mid-infrared optoelectronic devices such as interband cascade lasers and interband cascade detectors. Compared to n-type doped DBQW resonant tunneling structures, p-typed doped diodes show an enhanced peak-to-valley current ratio at cryogenic temperatures and room temperature. Besides the enhanced transport characteristics, p-type GaSb-based resonant tunneling diodes provide the following additional advantages over electron transport: GaSb is intrinsically p-type doped; the mobilities of electrons and holes are comparable; when deployed in the RTD photodetector scheme, the RTS can be easily integrated together with a lattice-matched narrow bandgap GaInAsSb semiconductor, or InAs/GaSb superlattice; since the band-offset almost exclusively takes place, photogenerated minority charge carriers can be captured for accumulation more efficiently and noise due to impact ionization processes will be reduced.

Supporting Information

Supporting Information is available from the Wiley Online Library or from the author.

Acknowledgements

The authors are grateful for financial support from the State of Bavaria, the German Ministry of Education and Research (BMBF) via the national project HIRT (FKZ 13XP5003B).

Received: ((will be filled in by the editorial staff))
Revised: ((will be filled in by the editorial staff))
Published online: ((will be filled in by the editorial staff))

References

[1] R. Tsu, L. Esaki, *Appl. Phys. Lett.* **1973**, *22*, 562.

[2] L. L. Chang, L. Esaki, R. Tsu, *Appl. Phys. Lett.* **1974**, *24*, 593.

[3] Jian Ping Sun, G. Haddad, P. Mazumder, J. N. Schulman, *Proc. IEEE* **1998**, *86*, 641.

[4] V. Aleshkin, L. Reggiani, *Phys. Rev. B* **2001**, *64*, 245333.

[5] Y. Blanter, M. Büttiker, *Phys. Rev. B* **1999**, *59*, 10217.

[6] V. Aleshkin, L. Reggiani, N. Alkeev, V. Lyubchenko, C. Ironside, J. Figueiredo, C. Stanley, *Phys. Rev. B* **2004**, *70*, 115321.

[7] M. Asada, S. Suzuki, N. Kishimoto, *Jpn. J. Appl. Phys.* **2008**, *47*, 4375.

[8] S. Suzuki, M. Asada, A. Teranishi, H. Sugiyama, H. Yokoyama, *Appl. Phys. Lett.* **2010**, *97*, 33.

[9] R. Izumi, S. Suzuki, M. Asada, in *2017 42nd Int. Conf. Infrared, Millimeter, Terahertz Waves*, IEEE, **2017**, pp. 1–2.

[10] B. Romeira, R. Avó, J. M. L. Figueiredo, S. Barland, J. Javaloyes, *Sci. Rep.* **2016**, *6*, 19510.

[11] B. Romeira, J. M. L. Figueiredo, J. Javaloyes, *Chaos An Interdiscip. J. Nonlinear Sci.* **2017**, *27*, 114323.

[12] J. Li, H. Guo, J. Liu, J. Tang, H. Ni, Y. Shi, C. Xue, Z. Niu, W. Zhang, M. Li, Y. Yu, *Nanoscale Res. Lett.* **2013**, *8*, 218.

[13] A. Pfenning, F. Hartmann, M. Rebello Sousa Dias, L. K. L. K. Castelano, C. Süßmeier, F. Langer, S. Höfling, M. Kamp, G. E. G. E. Marques, L. Worschech, V. Lopez-Richard, *ACS Nano* **2015**, *9*, 6271.

[14] P. England, J. E. Golub, L. T. Florez, J. P. Harbison, *Appl. Phys. Lett.* **1991**, *58*, 887.

[15] I. J. S. Coêlho, J. F. Martins-Filho, J. M. L. Figueiredo, C. N. Ironside, *J. Appl. Phys.* **2004**, *95*, 8258.

[16] B. Romeira, L. M. Pessoa, H. M. Salgado, C. N. Ironside, J. M. L. Figueiredo, *Sensors*

(Basel). **2013**, *13*, 9464.

[17] S. Höfling, A. Pfenning, R. Weih, A. Ratajczak, F. Hartmann, G. Knebl, M. Kamp, L. Worschech, in *Proc. SPIE - Int. Soc. Opt. Eng.* (Ed.: M. Strojnik), **2016**, p. 997306.

[18] H. Kroemer, *Phys. E Low-dimensional Syst. Nanostructures* **2004**, *20*, 196.

[19] B. Shanabrook, *... Opt. Sci. ...* **1999**, *3790*.

[20] C. Liu, T. Hughes, X.-L. Qi, K. Wang, S.-C. Zhang, *Phys. Rev. Lett.* **2008**, *100*, 236601.

[21] I. Knez, R.-R. Du, G. Sullivan, *Phys. Rev. Lett.* **2011**, *107*, 136603.

[22] F. Qu, A. J. A. Beukman, S. Nadj-Perge, M. Wimmer, B.-M. Nguyen, W. Yi, J. Thorp, M. Sokolich, A. A. Kiselev, M. J. Manfra, C. M. Marcus, L. P. Kouwenhoven, *Phys. Rev. Lett.* **2015**, *115*, 036803.

[23] G. Knebl, P. Pfeffer, S. Schmid, M. Kamp, G. Bastard, E. Batke, L. Worschech, F. Hartmann, S. Höfling, *Phys. Rev. B* **2018**, *98*, 041301.

[24] A. M. Hoang, G. Chen, A. Haddadi, M. Razeghi, *Appl. Phys. Lett.* **2013**, *102*, 011108.

[25] J. Faist, F. Capasso, D. L. Sivco, C. Sirtori, A. L. Hutchinson, A. Y. Cho, *Science (80-.).* **1994**, *264*, 553.

[26] Y. Yao, A. J. Hoffman, C. F. Gmachl, *Nat. Photonics* **2012**, *6*, 432.

[27] Y. Jiang, L. Li, R. Q. Yang, J. A. Gupta, G. C. Aers, E. Dupont, J.-M. Baribeau, X. Wu, M. B. Johnson, *Appl. Phys. Lett.* **2015**, *106*, 041117.

[28] I. Vurgaftman, R. Weih, M. Kamp, J. R. Meyer, C. L. Canedy, C. S. Kim, M. Kim, W. W. Bewley, C. D. Merritt, J. Abell, S. Höfling, *J. Phys. D. Appl. Phys.* **2015**, *48*, 123001.

[29] R. Weih, M. Kamp, S. Höfling, *Appl. Phys. Lett.* **2013**, *102*, 1.

[30] R. Q. Yang, *Superlattices Microstruct.* **1995**, *17*, 77.

[31] J. R. Meyer, I. Vurgaftman, R. Q. Yang, L. R. Ram-Mohan, *Electron. Lett.* **1996**, *32*, 45.

[32] R. Q. Yang, Z. Tian, J. F. Klem, T. D. Mishima, M. B. Santos, M. B. Johnson, *Appl. Phys. Lett.* **2010**, *96*, 063504.

[33] L. Lei, L. Li, W. Huang, J. A. Massengale, H. Ye, H. Lotfi, R. Q. Yang, T. D. Mishima, M. B. Santos, M. B. Johnson, *Appl. Phys. Lett.* **2017**, *111*, 113504.

[34] L. F. Luo, R. Beresford, W. I. Wang, *Appl. Phys. Lett.* **1989**, *55*, 2023.

[35] M. Kiledjian, J. Schulman, K. Wang, K. Rousseau, *Phys. Rev. B* **1992**, *46*, 12.

[36] R. Beresford, L. F. Luo, W. I. Wang, *Appl. Phys. Lett.* **1989**, *55*, 694.

[37] J. L. Jimenez, X. Li, W. I. Wang, *Appl. Phys. Lett.* **1994**, *64*, 2127.

[38] J. Jimenez, E. Mendez, X. Li, W. Wang, *Phys. Rev. B* **1995**, *51*, 7938.

[39] J. Jimenez, E. Mendez, X. Li, W. Wang, *Phys. Rev. B* **1995**, *52*.

[40] A. Pfenning, G. Knebl, F. Hartmann, R. Weih, A. Bader, M. Emmerling, M. Kamp, S. Höfling, L. Worschech, *Appl. Phys. Lett.* **2017**, *110*, 033507.

[41] A. Pfenning, G. Knebl, F. Hartmann, R. Weih, M. Meyer, A. Bader, M. Emmerling, L. Worschech, S. Höfling, *Appl. Phys. Lett.* **2017**, *111*, 171104.

[42] F. Hartmann, A. Pfenning, G. Knebl, R. Weih, A. Bader, M. Emmerling, M. Kamp, S. Höfling, L. Worschech, in *Proc. SPIE - Int. Soc. Opt. Eng.*, **2017**.

[43] I. Vurgaftman, J. R. Meyer, L. R. Ram-Mohan, *J. Appl. Phys.* **2001**, *89*, 5815.

[44] A. Vogt, A. Simon, J. Weber, H. . Hartnagel, J. Schikora, V. Buschmann, H. Fuess, *Mater. Sci. Eng. B* **1999**, *66*, 199.

[45] K. Vizbaras, M. Törpe, S. Arafin, M.-C. Amann, *Semicond. Sci. Technol.* **2011**, *26*, 075021.

[46] M. Hakala, M. J. Puska, R. M. Nieminen, *J. Appl. Phys.* **2002**, *91*, 4988.

[47] W. G. Hu, Z. Wang, B. F. Su, Y. Q. Dai, S. J. Wang, Y. W. Zhao, *Phys. Lett. A* **2004**, *332*, 286.

[48] S. Birner, S. Hackenbuchner, M. Sabathil, G. Zandler, J. A. Majewski, T. Andlauer, T. Zibold, R. Morschl, A. Trellakis, P. Vogl, *Acta Phys. Pol. A* **2006**, *110*, 111.

[49] A. C. Liapis, M. Y. Sfeir, C. T. Black, *Appl. Phys. Lett.* **2016**, *109*, 201101.

[50] F. Urbach, *Phys. Rev.* **1953**, *92*, 1324.

[51] P. Van Mieghem, *Rev. Mod. Phys.* **1992**, *64*, 755.

[52] V. Rakovics, A. L. Tóth, B. Podör, C. Frigeri, J. Balázs, Z. E. Horváth, *Mater. Sci. Eng. B* **2002**, *91–92*, 83.

[53] S. R. Johnson, T. Tiedje, *J. Appl. Phys.* **1995**, *78*, 5609.

[54] K. Shim, *J. Appl. Phys.* **2013**, *114*, 203703.

[55] A. Pfenning, F. Hartmann, M. Rebello Sousa Dias, F. Langer, M. Kamp, L. K. L. K. Castelano, V. Lopez-Richard, G. E. G. E. Marques, S. Höfling, L. Worschech, *Appl. Phys. Lett.* **2015**, *107*, 081104.

[56] A. Pfenning, F. Hartmann, F. Langer, M. Kamp, S. Höfling, L. Worschech, *Nanotechnology* **2016**, *27*, 355202.

[57] P. W. Park, H. Y. Chu, S. G. Han, Y. W. Choi, G. Kim, E.-H. Lee, *Appl. Phys. Lett.* **1995**, *67*, 1241.

[58] A. Pfenning, F. Hartmann, F. Langer, M. Kamp, S. Höfling, L. Worschech, in *Proc. SPIE - Int. Soc. Opt. Eng.* (Ed.: M. Strojnik), **2016**, p. 997307.

[59] F. Rothmayr, A. Pfenning, C. Kistner, J. Koeth, G. Knebl, A. Schade, S. Krueger, L. Worschech, F. Hartmann, S. Höfling, *Appl. Phys. Lett.* **2018**, *112*, DOI 10.1063/1.5025531.

[60] J. Schulman, H. J. De Los Santos, D. H. Chow, *IEEE Electron Device Lett.* **1996**, *17*, 220.

[61] R. Ferrini, M. Patrini, S. Franchi, *J. Appl. Phys.* **1998**, *84*, 4517.

[62] M. Muñoz, K. Wei, F. H. Pollak, J. L. Freeouf, G. W. Charache, *Phys. Rev. B* **1999**, *60*, 8105.

[63] W. Huang, L. Li, L. Lei, J. A. Massengale, R. Q. Yang, T. D. Mishima, M. B. Santos, *J. Appl. Phys.* **2018**, *123*, 113104.

[64] I. E. Gordon, L. S. Rothman, C. Hill, R. V. Kochanov, Y. Tan, P. F. Bernath, M. Birk, V. Boudon, A. Campargue, K. V. Chance, B. J. Drouin, J.-M. Flaud, R. R. Gamache, J. T. Hodges, D. Jacquemart, V. I. Perevalov, A. Perrin, K. P. Shine, M.-A. H. Smith, J. Tennyson, G. C. Toon, H. Tran, V. G. Tyuterev, A. Barbe, A. G. Császár, V. M. Devi, T. Furtenbacher, J. J. Harrison, J.-M. Hartmann, A. Jolly, T. J. Johnson, T. Karman, I. Kleiner, A. A. Kyuberis, J. Loos, O. M. Lyulin, S. T. Massie, S. N. Mikhailenko, N. Moazzen-Ahmadi, H. S. P. Müller, O. V. Naumenko, A. V. Nikitin, O. L. Polyansky, M. Rey, M. Rotger, S. W. Sharpe, K. Sung, E. Starikova, S. A. Tashkun, J. Vander Auwera, G. Wagner, J. Wilzewski, P. Wcisło, S. Yu, E. J. Zak, *J. Quant. Spectrosc. Radiat. Transf.* **2017**, *203*, 3.

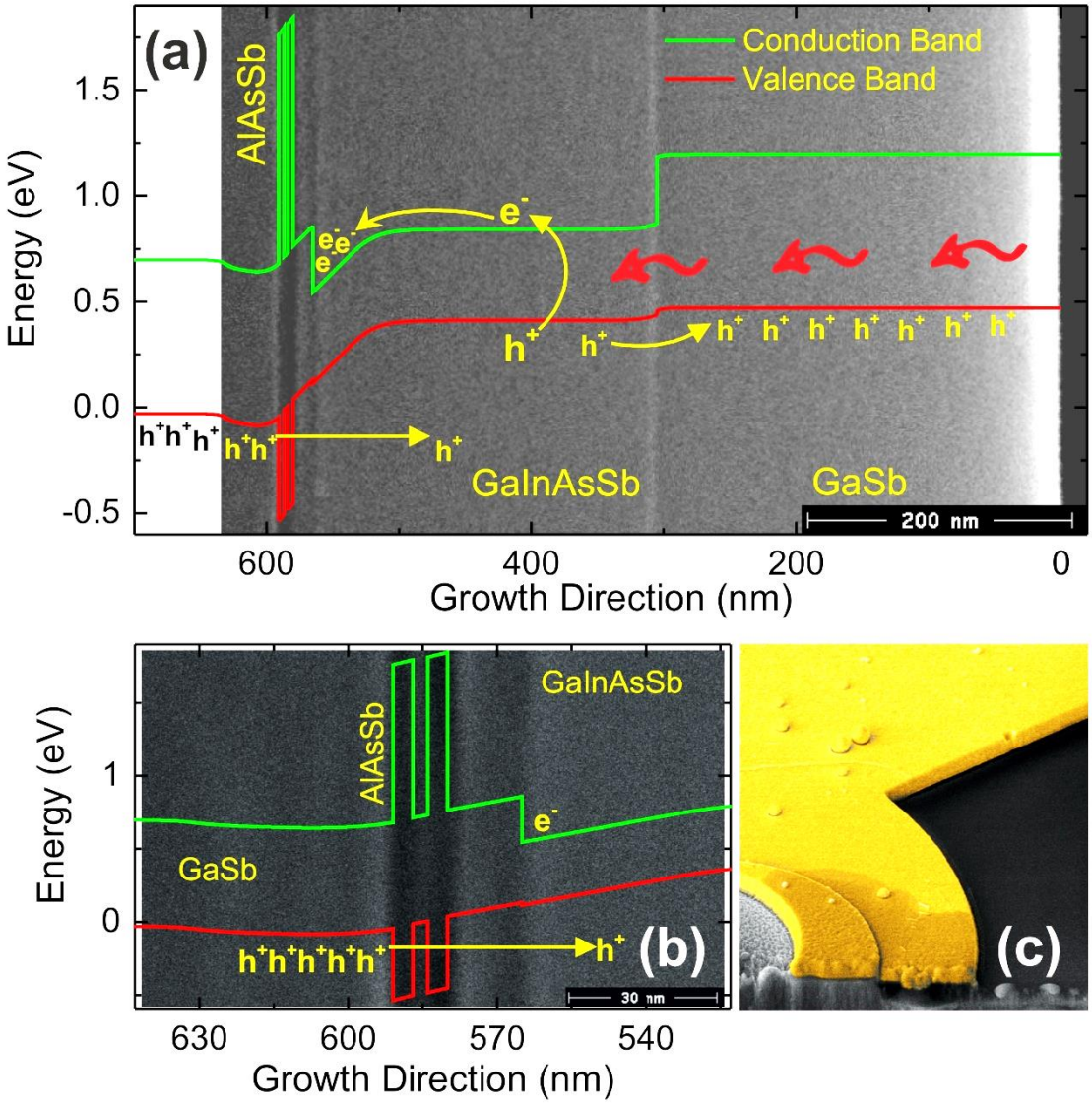

Figure 1. Sample design and illustration of the operation principle of a p-type doped RTD photodetector. Simulations and electron microscopy images are from sample *RTD-p1*. **(a)** Simulated conduction band (CB, green) and valence band (VB, red) profiles for an applied bias voltage of $V = -0.5$ V. CB and VB profiles are underlaid with a cross-sectional scanning electron microscopy (SEM) image of semiconductor layer structure. **(b)** High-resolution SEM image of the resonant tunneling structure. **(c)** Colored SEM image of the RTD mesa structure and Au-ring shaped contact.

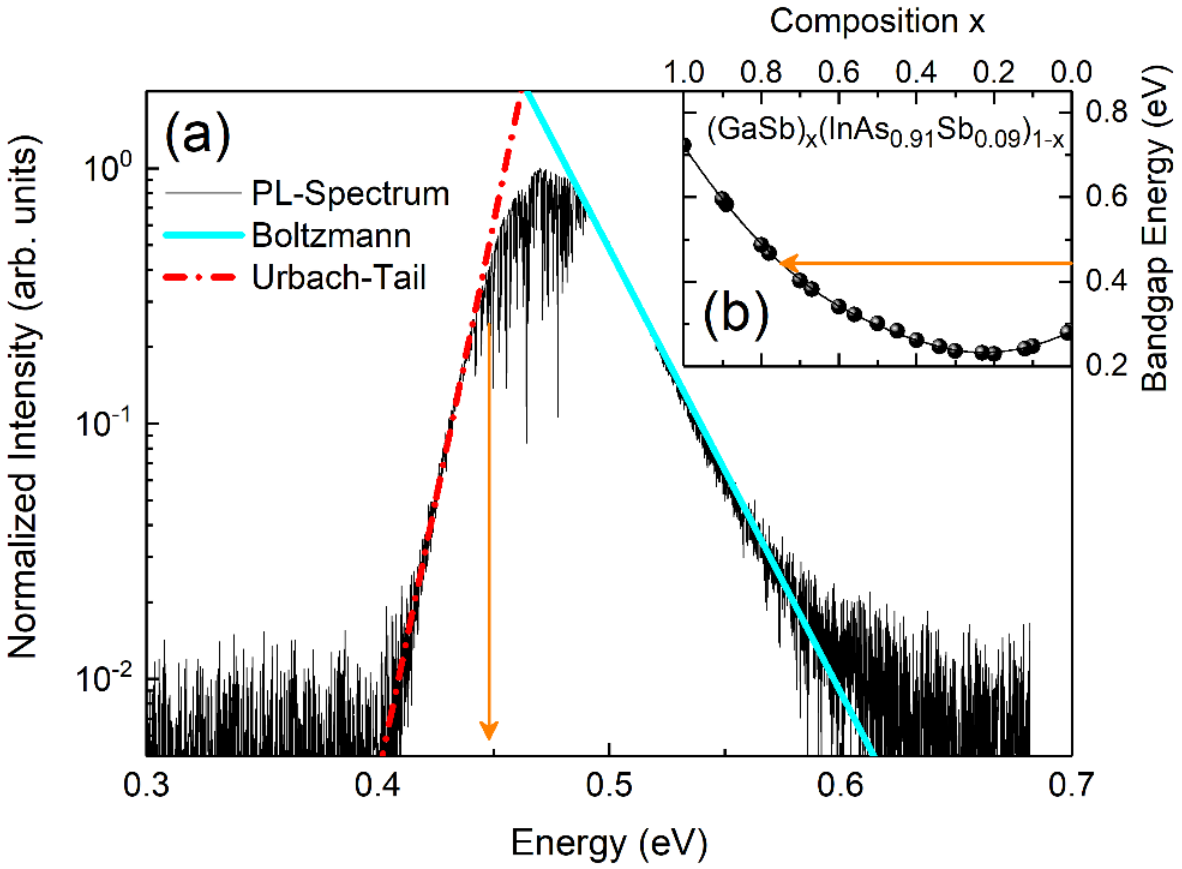

Figure 2. (a) Fourier-transform infrared (FTIR) photoluminescence (PL) spectrum of the studied RTD, measured at a temperature of $T = 20$ °C. From the low-energy side increase, an Urbach-parameter of $E_U = 10$ meV is extracted. The high-energy side decay is determined by a Boltzmann's distribution (solid blue line). The bandgap energy of $E_{Gap} = (447 \pm 5)$ meV is indicated by the orange arrow. The dashed red line represents Urbach's band-tail. **(b)** Bandgap energy versus composition of the quaternary GaInAsSb lattice-matched to GaSb after *Shim.* [54].

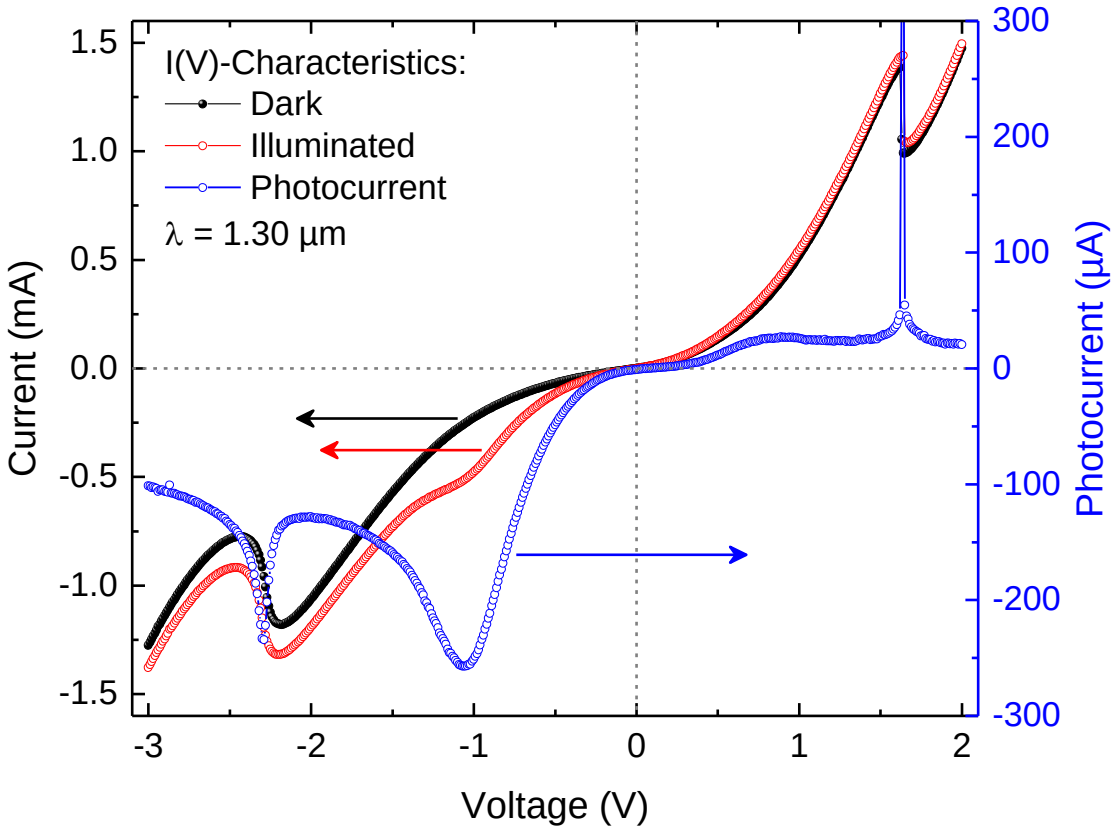

Figure 3. I(V)-characteristic of *RTD-p1* for a diode with diameter $d = 12$ µm measured in the dark (black) and under illumination with laser light of the wavelength $\lambda = 1.30$ µm (red). The incident light power is $P \lesssim 0.7$ mW. The corresponding photocurrent-voltage relation $I_{Ph}(V)$ is shown in blue. The asymmetric photocurrent-voltage characteristic is a clear indicator for accumulation of photogenerated minority charge carriers at the RTS.

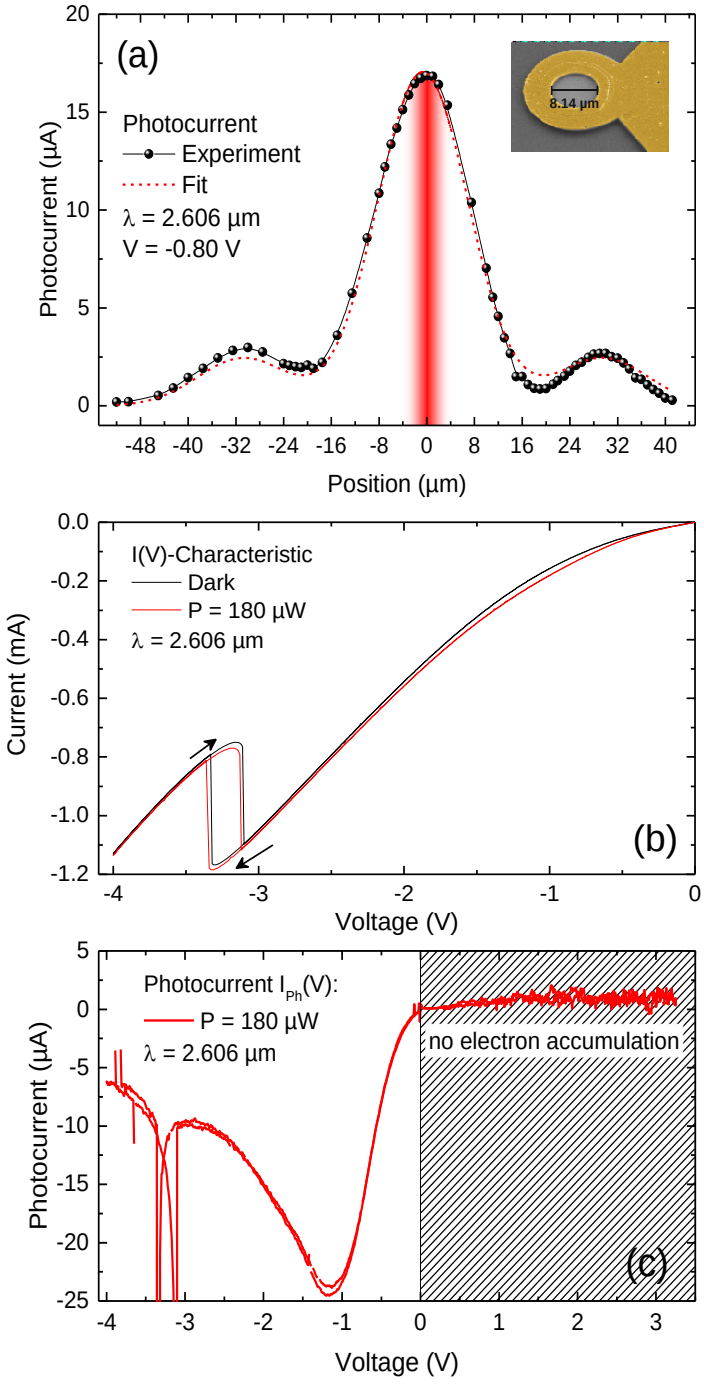

Figure 4. Mid-infrared photoresponse at room temperature for illumination with a mono-mode diode laser of the wavelength $\lambda = 2.606$ µm. **(a)** Cross-section of the laser intensity profile given by the photocurrent (black spheres) as a function of diode position. The inset shows a colored SEM image of an RTD mesa structure with diameter of nominally $d = 12$ µm and Au-ring shaped contact. The optically accessible area has a diameter of $d = 8.14$ µm. From the best fit function (red dashed line) of the convolution, the fraction of light power incident on the RTD is calculated to be about 5.8 %. **(b)** I(V)-characteristics in the dark (black) and under illumination with $\lambda = 2.606$ µm and $P \simeq 180$ µW. The bistability is due to a series resistance of $R = 1.0$ kΩ. **(c)** Photocurrent-voltage characteristics $I_{Ph}(V)$ for an incident light power of $P \simeq 180$ µW. Only for negative bias voltages, photogenerated electrons can accumulate in the vicinity of the RTS and modulate the tunneling current via Coulomb interaction.

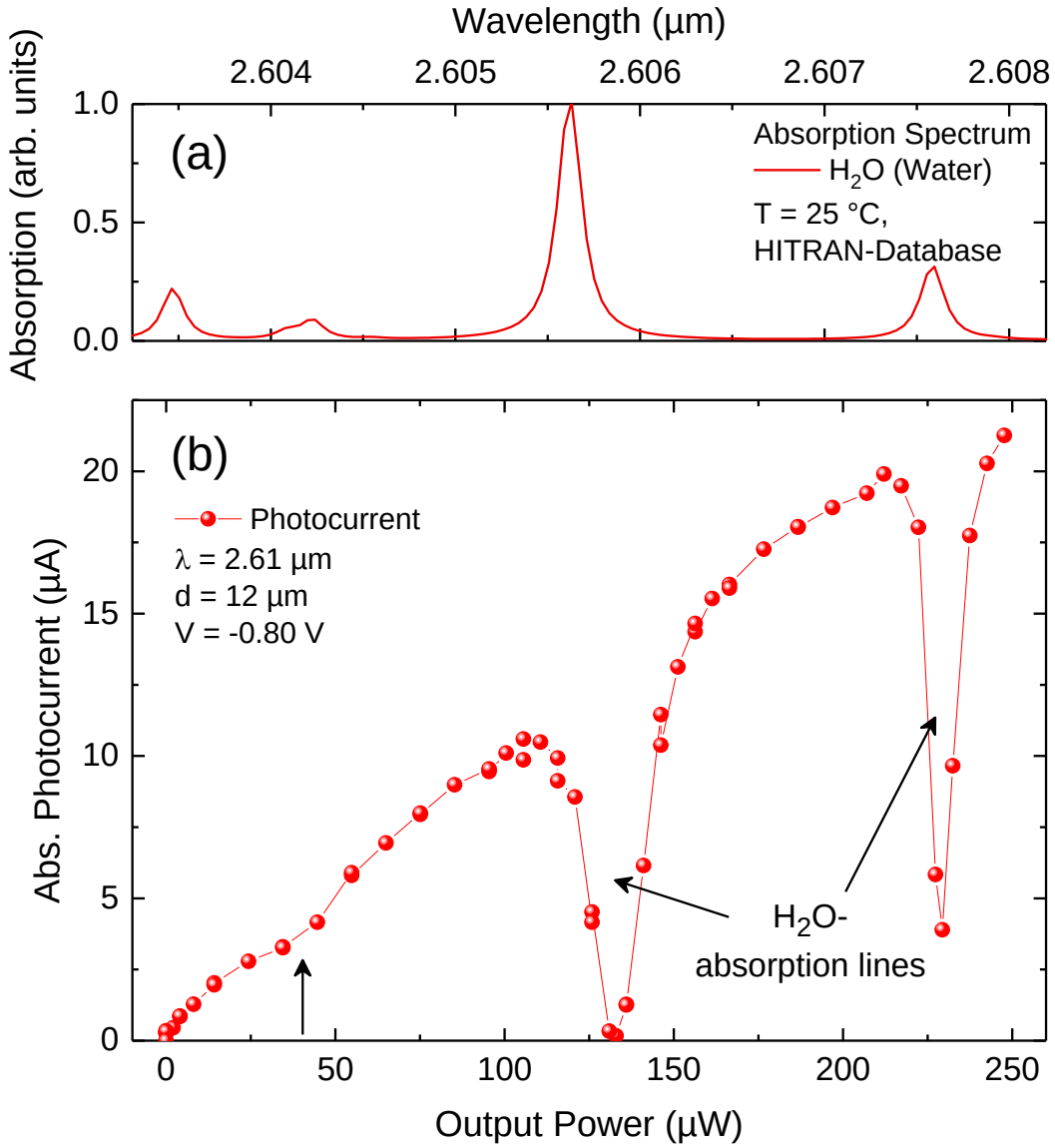

Figure 5: (a) Water absorption spectrum at $T = 25$ °C at around 2.61 µm. The data is taken from the HITRAN database.[64] **(b)** Absolute photocurrent as a function of the laser output power incident on the optical aperture of the Au-ring shaped contact. The output power is tuned via the diode current. Due to Joule heating, the emission wavelength undergoes a red-shift with increasing output power. When the emission wavelength crosses a water absorption line, a drop in the photocurrent is observed. These local minima are indicated by black arrows.

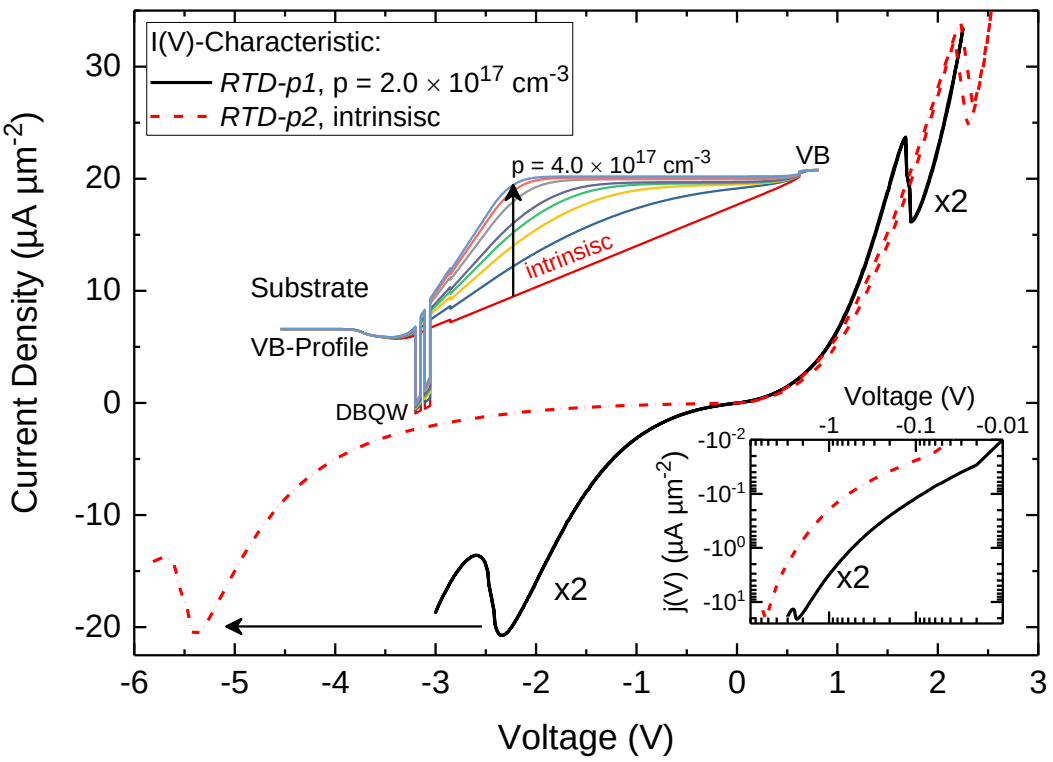

Figure 6. Current density-voltage (j(V)-) characteristics of the p-type doped RTD photodetector for two different doping concentrations of the GaInAsSb absorption layer. The j(V)-characteristic of *RTD-p1* is shown as solid black line and is multiplied by a factor of two. The j(V)-characteristic of *RTD-p2* is shown as dashed red line. The first inset in the upper middle of the figure shows the simulated VB profile for increasing doping concentrations of the GaInAsSb absorption layer from intrinsic to $p = 4.0 \times 10^{17}$ cm^{-3}. The second inset in the lower right shows the j(V)-characteristic for negative bias voltages on the log-log scale. The comparison demonstrates that the shift of the resonance with lower doping of the absorption layer can be attributed to a lower RTD leverage factor.

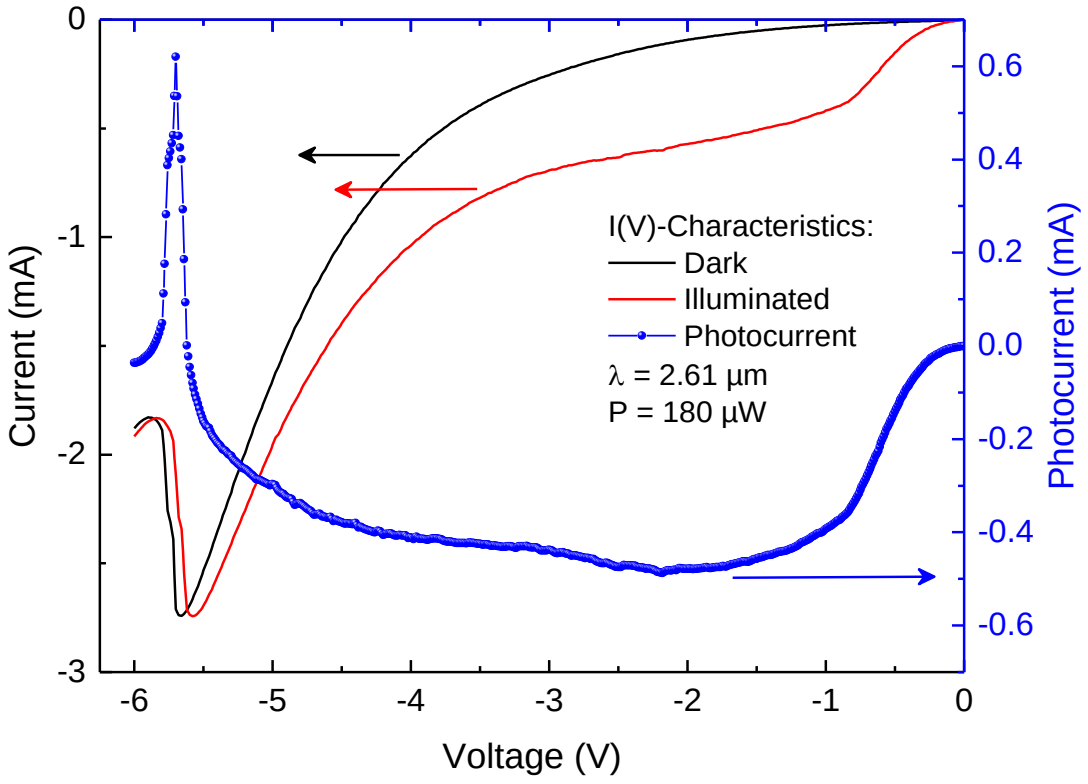

Figure 7: I(V)-characteristics of *RTD-p2* taken in the dark (black) and under illumination with laser light of the wavelength $\lambda = 2.61$ µm and an incident light power of $P \simeq 180$ µW. Under illumination the I(V)-characteristic shifts towards smaller voltages, which causes a photocurrent to arise. The photocurrent-voltage $I_{Ph}(V)$is shown as blue spheres. Compared to

The table of contents entry (50-60 words)

Antimony-based resonant tunneling diodes (RTDs) are a promising alternative for mid-infrared (MIR) photodetectors with gain at considerably low operation voltages. Their capability is demonstrated in a tunable diode laser absorption spectroscopy (TDLAS) experiment. The possibility to exploit hole transport by p-type doping provides further advantages and can also be applied to alternative material systems such as GaAs or InP.

Mid-infrared, photodetector, resonant tunneling diode, RTD, holes, GaSb

Andreas Pfenning, Fabian Hartmann,** Robert Weih, Monika Emmerling, Lukas Worschech, and Sven Höfling*

p-type doped AlAsSb/GaSb resonant tunneling diode photodetector for the mid-infrared spectral region

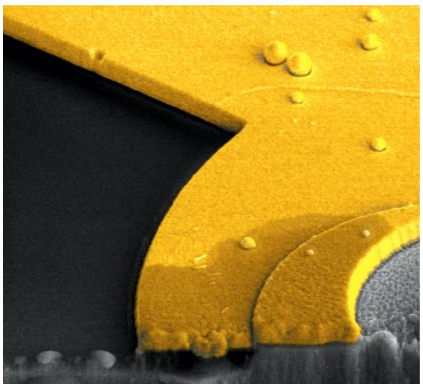

Supporting Information

p-type doped AlAsSb/GaSb resonant tunneling diode photodetector for the mid-infrared spectral region

Andreas Pfenning, Fabian Hartmann, Robert Weih, Monika Emmerling, Lukas Worschech, and Sven Höfling*

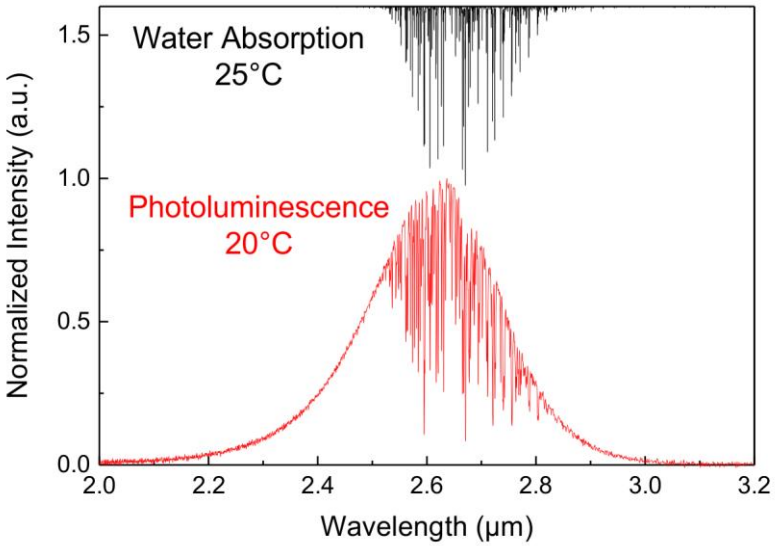

Figure S1. Normalized photoluminescence (red) taken at $T = 20$ °C and water absorption lines at $T = 25$ °C. The water absorption lines are reproduced from datasets of the HITRAN database.[64] The absorption lines of the HITRAN absorption spectrum are slightly red-shifted compared to the PL spectrum, which is due to its slightly elevated temperature.